



An experimental investigation of the effect of owl-inspired velvety coating on trailing edge noise

Peng Zhou^{*}, Go Nam Lui[†] and Xin Zhang[‡]
*The Hong Kong University of Science and Technology
Clear Water Bay, Kowloon, Hong Kong SAR, China*

Many owl species have three adaptations on their wings that are responsible for their quiet flight: the comb-like serrations at the leading edge, the soft fringes at the trailing edge, as well as the velvety structure on the upper wing surface. This study was inspired by the third feature. An experimental investigation was conducted at the HKUST low-speed wind tunnel, UNITED, to study the effect of artificial velvety structure on the boundary layer flow, as well as the trailing edge noise of a flat plate model. The chord-based Reynolds number ranged between 160,000 to 300,000. Turbulent strips were used to suppress instability noise. Four different velvety coatings with different hair dimensions were tested. The induced noise source distribution and the noise level were acquired by a 56-channel microphone array. Acoustic measurements show that all the tested velvety coatings can reduce the trailing edge noise above a critical chord-based Strouhal number, which depends on both the hair length and the location of the coating. However, the velvety coatings also increases the induced noise below that Strouhal number. The coating thickens the boundary layer, elevates the overall turbulent spectrum in the boundary layer at all frequencies, but reduces the velocity fluctuation in the vicinity of the trailing edge. If the acoustic measurement results were extended to the case of owls' flight (below 10 m/s), then the velvety coating can reduce noise above a critical frequency that is well below 2 kHz, which is the lower hearing threshold of owls' prey.

I. Introduction

Trailing edge noise is a major component of the airframe noise at the clean configuration, and determines the lower bound of the aircraft noise [1]. Edge scattering is the primary mechanism of trailing edge noise that transforms the flow energy in the turbulent boundary layer to the out-propagating acoustic energy [2, 3]. A noticeable reduction of the trailing edge noise is challenging, since a significant modification of the aircraft geometry would be required to minimise the edge scattering effect [1]. To encounter this challenge, people start to seek inspirations from nature. The quiet flight of owls, which is believed to result from millions of years of evolution, has been attracting the attention of scientists and engineers for more than 80 years [4]. Most owls are nocturnal. Their prey, typically rodents and lagomorphs [5], have acute hearing above 2 kHz [6, 7]. Besides, owls themselves use binaural hearing to locate the prey [8], with the most accurate hearing range above 2 kHz as well [9]. Therefore, it can be conjectured that owls have special adaptations that reduce the high-frequency components of their flight noise.

Several previous noise measurements have indicated the quiet flight capabilities of owls. Early studies [6, 10, 11], however, did not account for the low flight speed of owls, which is a crucial parameter for the sound level of flow generated noise [12]. Sarradj *et al.* [13] carefully conducted a field noise measurement of different species of birds, including a barn owl. They concluded that after velocity scaling, the barn owl still generates 3–8 dB less flight noise compared to other birds with similar size, at a frequency above 1.6 kHz. This proved that owls' adaptations, apart from the low flight speed, are also responsible for owls' silent flight.

The peculiarities of owl wings were first summarised by Graham [4] as the comb-shaped leading edge serrations, soft trailing edge fringes and the velvety upper wing surface. Limited study was focused on the underlying mechanism of the last property, and currently, there are no applications based on the velvety structure of the owl feathers [14]. Several hypotheses have been proposed to explain the function of this structure:

- 1) The velvety structure may reduce feather sliding noise. Graham [4] proposed that this structure may reduce the noise generated when the feather slides across each other. This hypothesis is highly possible since the velvet

^{*}PhD student, Department of mechanical and aerospace engineering.

[†]PhD student, Department of mechanical and aerospace engineering.

[‡]Swire professor of aerospace engineering and chair professor, Department of mechanical and aerospace engineering. Email: aexzhang@ust.hk

- length is increased in the feather overlapping region [15, 16].
- 2) The velvety structure may absorb noise. Chen *et al.* [16] conjectured that the velvety structure acts as a porous sound absorber. The measured sound absorption coefficient of an eagle owl feather was higher than that of a common buzzard feather. Vad *et al.* [17] attached a commercially available velvet on a rectilinear airfoil to mimic the velvety structure, and observed up to 1.4 dBA sound reduction of the trailing edge noise at $Re \approx 300,000$. In particular, they observed over 5 dB noise reduction near 1600 Hz. They attributed the noise reduction solely to the sound absorption property of the velvet.
 - 3) The velvety structure may modify the global flow structure. Klän *et al.* [18] and Winzen *et al.* [19] conducted wind tunnel experiments for wing models covered with artificial velvet surfaces, with fibre length and density comparable to that of owl wings. They discovered that at low Reynolds number, the velvet surface was able to delay the flow separation at the suction side of the highly cambered wing. The authors speculated that the reduction of separation contributes to the low flight noise of owls.
 - 4) The velvety structure may modify the edge scattering process. Clark *et al.* [20, 21] speculated that the velvety structure may lift the boundary layer away from the surface, thus reduce the trailing edge scattering efficiency. They used finlet fences near the trailing edge to mimic the function of the velvety structure, and observed an up to 10 dB noise reduction near 3 kHz, at $Re = 3 \cdot 10^6$, with relatively small adverse aerodynamic effect. However, the functional equivalence between the velvety structure and the finlet fence was not proved.
 - 5) The velvety structure may manipulate the near wall turbulent structure. Lilley [7] suggested a bypass turbulent cascade mechanism: the thin and compliant filaments in the velvety structure may absorb energy from small-scale turbulent eddies, thus reduce the cut-off frequency of the turbulent cascade process, which is corresponding to the Kolmogorov time scale without the presence of velvet structures. There is, however, no experimental proof for this hypothesis.

Since biological structures usually possess multi-functionality [22], it is possible that the velvety structure on owl feathers may contribute to more than one of the above-mentioned functionalities.

The aim of the present research is to systematically study the effect of owl-inspired velvety coating on the trailing edge noise by anechoic wind tunnel measurements. A flat plate model is selected to remove the effect of surface curvature and the possible flow separation. In the next section, more details of the velvety structures are elaborated. The experimental setup, including artificial velvety coating preparation, phased microphone array setup, as well as hot wire anemometry, is then described. The effect hair dimensions and the location of velvety coatings on the trailing edge noise and the boundary layer flow is investigated. Finally, the aforementioned hypotheses 2), 4) and 5) were evaluated.

II. The velvety structure of owl feathers

To study the effect of the velvet structure of owl feathers on the flight noise, as well as to artificially replicate the structure, the structural, mechanical and acoustical properties of the velvet need to be acquired. The 10th primary feather of an eagle owl was observed using the JEOL-6390 Scanning Electron Microscope in the HKUST Material Characterization and Preparation Facility. As clearly shown in Figure 1, the velvety structure is only prominent at the inner vane of the proximal portion of the feather. The velvety structure is composed of elongated pennula, with a length of approximately 1.5 mm and a diameter of about 4 μm . The pennula bend and become parallel to the feather surface at the tip. The velvety structure becomes thinner and sparser near the trailing edge. At the inner vane of the distal portion of the feather, the velvety structure is much less prominent than that at the proximal part. The pennulum here has a length of approximately 0.5 mm, and a diameter of about 8 μm . At the outer vane, the feather is characterized by thick and stiff fibres of diameter about 25 μm . The observed morphological characteristics of the velvety structure are in agreement with the previous studies [15, 21]. The measured pennula length is slightly larger than that from Bachmann *et al.* [15], possibly due to the different owl species being used. However, the observed pennula diameter is smaller, indicating a more flexible velvety structure.

Due to the limitation of testing facilities, the mechanical properties of the velvety structure were not measured. Instead, the relevant data in the literature were used. Bachmann *et al.* [23] measured the Young's modulus of the rachis of barn owls' feathers using nanoindentation method and two-point bending test. The rachis is composed of keratin, same as the velvet structure. The measured Young's modulus was 4–7 GPa, depending on the test sample locations. Recently, the mechanical properties of long-eared owl feather components in different length scales were carefully tested by Gao *et al.* [24], using a micro-tensile testing system. They discovered a strong size dependence of the Young's modulus: the measured Young's modulus was 1–2 GPa for the barbules (base part of the pennulum), while 8–9 GPa for the rachis.

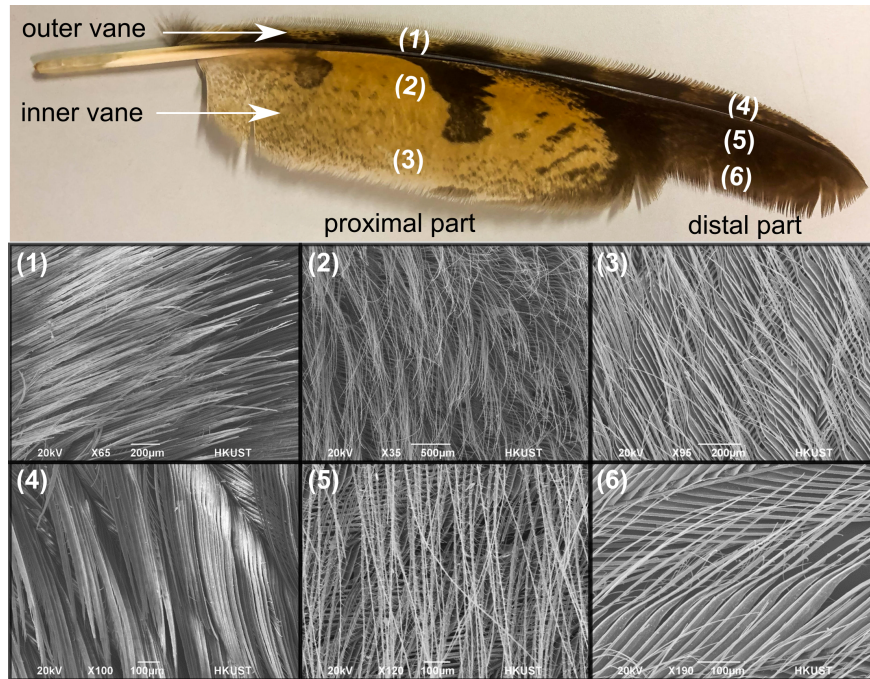


Fig. 1 SEM pictures of six samples located on different parts of an eagle owl's 10-th primary feather. Upper: locations of feather samples for SEM observation. Lower: SEM image of (1) Outer vane, proximal part. (2) Inner vane, proximal part, far from the trailing edge. (3) Inner vane, proximal part, close to the trailing edge. (4) Outer vane, distal part, (5) Inner vane, distal part, far from the trailing edge. (6) Inner vane, distal part, close to the trailing edge.

In order to verify if the velvety structure on the owl feather has significant contribution to owls' silent flight, the sound absorption coefficient of an eagle owl feather was measured by the Brüel & Kjær type 4206 impedance tube kit, with a frequency range of 500–6,000 Hz. Two samples were cut from the feather into circular shape with diameter of 29 mm: one is at the inner vane of the proximal part of the feather, where the velvet structure is thick and dense; the other is at the inner vane of the distal part of the feather, where the velvety structure is thinner and sparser. Figure 2 shows that although the proximal part of the feather gives a slightly higher absorption coefficient at high frequency, the magnitude of the absorption coefficient of both samples is small - below 0.11 within the frequency range. This result is similar to the measurement by Chen *et al.* [16]. With a normal incident sound wave, this corresponds to a maximum of 0.5 dB noise reduction. Since during owls gliding flight, there can only be up to two layers of primary feather overlapping at the wing surface, the overall sound absorption is not likely to be largely increased compared to a single layer of feather. Therefore, the sound absorption by the velvety structure may not be the primary contributor to owls' silent flight. In this study, only the dimension and the mechanical properties of the velvety structure of owl feathers are selected as the criteria for the artificial velvety structure. The detailed test setup will be introduced in the next session.

III. Experimental setup

A. Anechoic wind tunnel facility

The flat plate trailing edge noise measurements and flow measurements were conducted in an anechoic wind tunnel, Ultra-quiet Noise Injection Test and Evaluation Device (UNITED) [25, 26], at The Hong Kong University of Science and Technology. The open-jet test section was used for this study. The wind tunnel has a square cross-section with a side length of 0.4 m. The flow speed can vary from 10 m/s to 70 m/s, and the inflow turbulence intensity is lower than 0.27% for the speed range of 16-30 m/s. The test section is enclosed by a half-anechoic chamber with a cut-off frequency of 200 Hz, whose dimensions are 3.3 m (L) × 3.1 m (W) × 2.0 m (H).

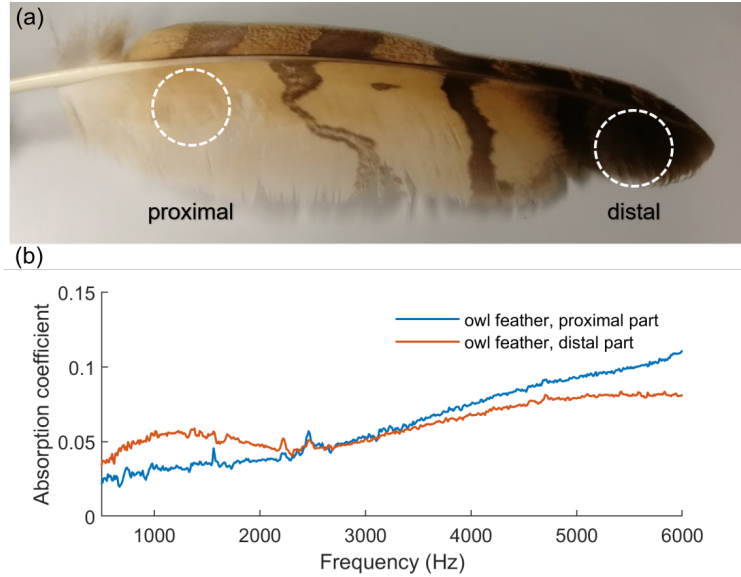


Fig. 2 The sound absorption property of the owl feather. (a) The locations of feather samples for sound absorption measurement. (b) The measured absorption coefficient of different feather samples.

B. Flat plate model

A flat plate model was used in this study to simplify the flow condition. The model has a chord of 150 mm, a span of 400mm and a thickness of 6mm. The cross-sectional geometry of the model is shown in Fig. 3(a). The model has an elliptical leading edge with an aspect ratio of 4:1 and a symmetric trailing edge with a contraction angle of 12° . The thickness at the trailing edge is measured to be less than 0.2 mm. A fillet with 500 mm radius was added between the flat section and the contraction section of the model to prevent flow separation, which typically occurs for a bevelled type trailing edge [27]. Two acrylic end plates were used to hold the flat plate model to maintain the flow two-dimensionality and to prevent noise associated with the free shear layer. The angle of attack of the flat plate was set to be 0° . In order to suppress the laminar boundary layer-instability noise, a serrated trip strip with a thickness of 0.3 mm was attached to both sides of the model, occupying the 12% to 20% portion of the chord. The free stream velocity U_∞ in this experiment ranges between 16 m/s to 30 m/s, corresponding to a chord based Reynolds number between 1.6×10^5 and 3.0×10^5 .

C. Artificial velvety coating

Artificial velvety coatings were fabricated to mimic the dimensional and mechanical properties of the velvety structure on owls' feather. The velvety coating contains nylon fibres with a Young's modulus of 2.5–3.9 GPa, which is close to that of owls' velvety structure [24]. Four different types of velvety coating with varying hair dimensions, as shown in Table 1, were fabricated. The hair diameter is slightly larger than that in the owls' velvet structure. The fibres were attached to a 0.05 mm thick PET substrate film perpendicularly through electrostatic flocking technique. The coated film was then precisely cut and adhered to the flat plate model on both sides. Two different coating sizes were tested in this experiment. The first one has the same span with the flat plate model, and occupies the 20% to 100% portion of the chord of the flat plate model, right after the trip strip. The second one has the same span and occupies 36.7% of the chord. This size allows the coating to be adhered at different chordwise locations of the model.

Table 1 Dimensions of hairs in the artificial velvety coating.

Sample name	H0.3	H0.7	H1.0	H1.5
Hair length (mm)	0.3	0.7	1.0	1.5
Hair diameter (μm)	10	13	13	26

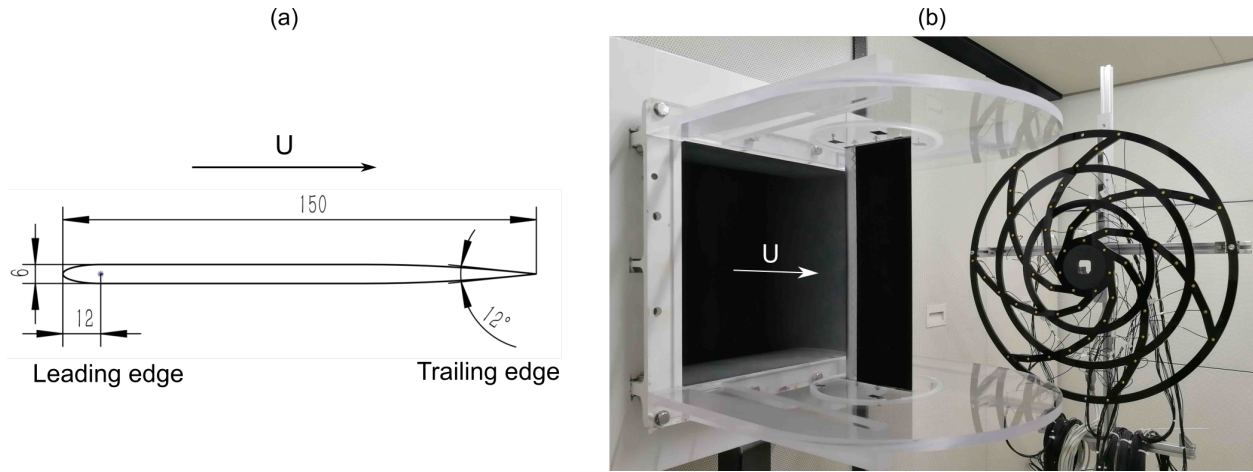


Fig. 3 The wind tunnel experimental setup. (a) The dimensions of the cross section of the flat plate model. All numbers are in millimeters. (b) The acoustic measurement setup, including the end plates, flat plate model with velvety coating, and the microphone array.

D. Phased microphone array measurement

A planar phased microphone array consisting of 56 1/4 inch Brüel & Kjær type 4957 microphones, as shown in Fig. 3(b), was used to acquire the sound source distribution. Each microphone has a flat frequency response within 50–10,000 Hz, and was calibrated by a Brüel & Kjær type 4231 sound calibrator. The microphones are located in 7 spiral arms to reject spatial aliasing [28]. The microphone plane was set parallel to the flow direction with a distance of 0.728 m from the flat plate trailing edge. The centre of the microphone array was aligned with the centre of the flat plate trailing edge. Four 24-bit National Instrument PXIe-4497 cards were used to record the microphone data simultaneously. The sampling frequency was 48 kHz, and the number of data points per channel for each measurement was 409,600. Fast Fourier Transformation was used to transform the data into the frequency domain. The data were divided into 100 Hanning windows with a window size of 4,096, giving a frequency resolution of 11.72 Hz. The cross spectra matrix was obtained by averaging the cross spectra of 100 blocks. The conventional beamforming algorithm with diagonal removal was used to calculate the source distribution within the model plane. The sound refraction effect by the jet shear layer was corrected using the average Mach number method [29]. Because of the distributed nature of the trailing edge noise, a source integration method with an array correction function was used to quantify the absolute trailing edge noise strength [30].

E. Flow measurement

Hot-wire anemometry was used to acquire the velocity profile as well as the turbulence characteristics of the boundary layer in the vicinity of the trailing edge. A Dantec type 55P11 single-sensor hot-wire probe, connected with Dantec StreamLine Pro Anemometer System, was used. The probe was placed at the mid-span location, and has a streamwise distance to the flat plate trailing edge of 0.7 mm. The direction of the hot-wire is parallel to the trailing edge. The probe was installed on a Dantec traverse system with a positional accuracy of 6.25 μm . For each measurement, the probe scanned across the wake within $y = \pm 10$ mm from the trailing edge, with a step size of 0.25 mm. Velocities were sampled at a frequency of 50,000 Hz with a sample time of 10 s. For spectrum calculation, the data were divided into 199 Hanning windows with a window size of 5,000 and an overlapping ratio of 50%. This gives a frequency resolution of 10 Hz.

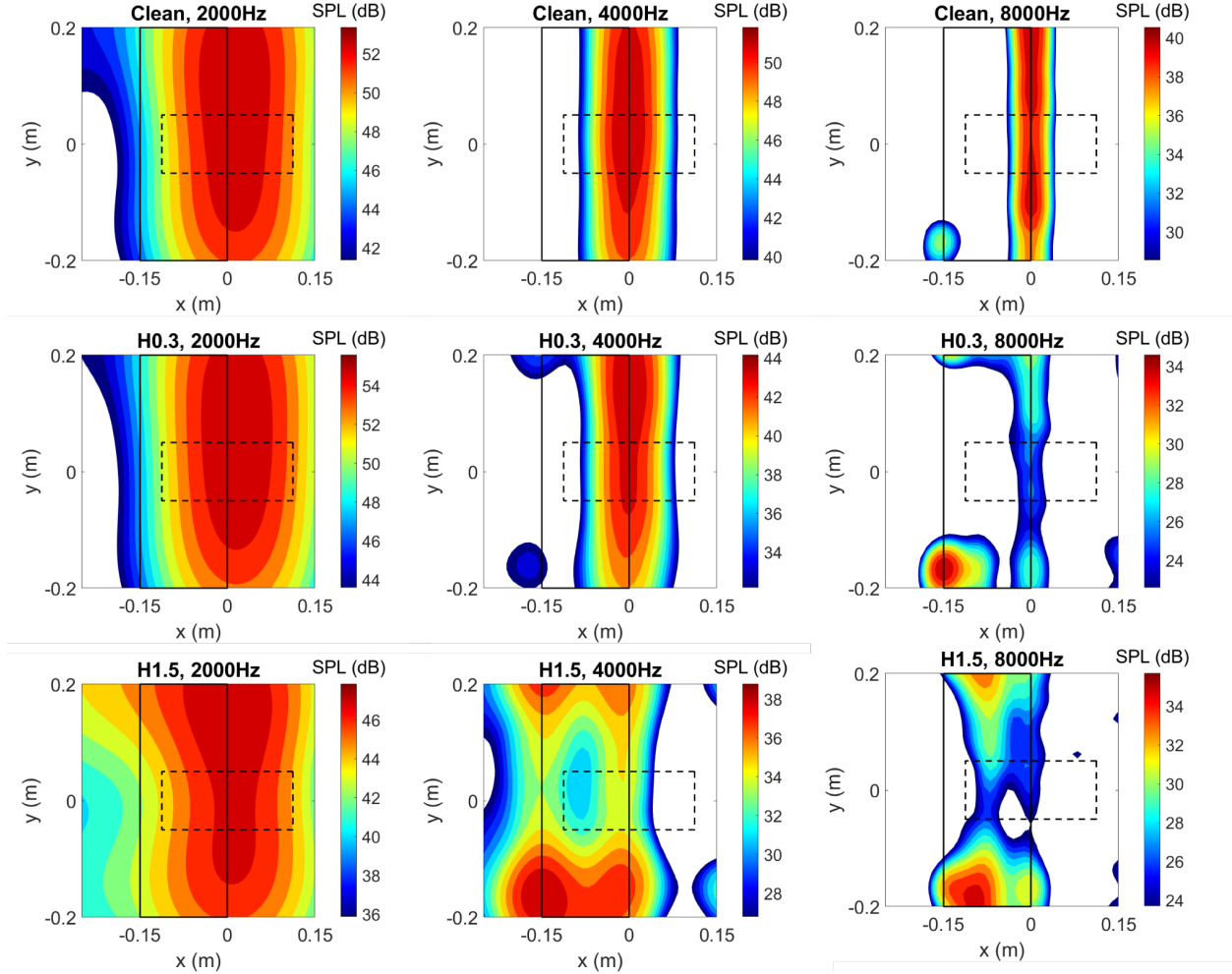


Fig. 4 Comparison of the 1/3-octave acoustic images at three different frequencies. Upper row: clean flat plate model; middle row: flat plate model with 0.3 mm velvety coating (H0.3); lower: flat plate model with 1.5 mm velvety coating (H1.5). Flow direction is from left to right. The solid contour indicates the flat plate model, and the dashed contour indicates the source integration region. The color scale is adjusted in each plot, and the dynamic range is 12 dB.

IV. Results and discussions

A. Noise measurement results

1. Effect of the thickness of the velvety structure

To study the effect of the hair dimension of the velvet structure on the trailing edge noise, four types of velvety coatings, as listed in Table 1 were tested. The velvety coatings have a chordwise coverage from 20% to 100%. The acoustic images of three configurations are shown at 20 m/s are shown in Fig. 4: the clean configuration, the model with 0.3 mm velvety coating (H0.3) and the model with 1.5 mm velvety coating (H1.5). The results are shown in one-third octave bands with centre frequency at 2,000, 4,000 and 8,000 Hz, respectively. For the clean model, it is apparent that the dominant noise sources at selected frequencies are distributed at the trailing edge. Due to the limited array aperture, the reconstructed source distribution can spread beyond the leading edge below 2,000 Hz. The source distribution for the test model with H0.3 velvety coating at 2,000 Hz is similar to that of the clean configuration, and the source strength is elevated by 2 dB. At 4,000 and 8,000 Hz, the H0.3 velvety coating results in an 8–10 dB reduction in source strength in the trailing edge region, compared to the clean configuration. Due to this reduction, the model-end plate junction

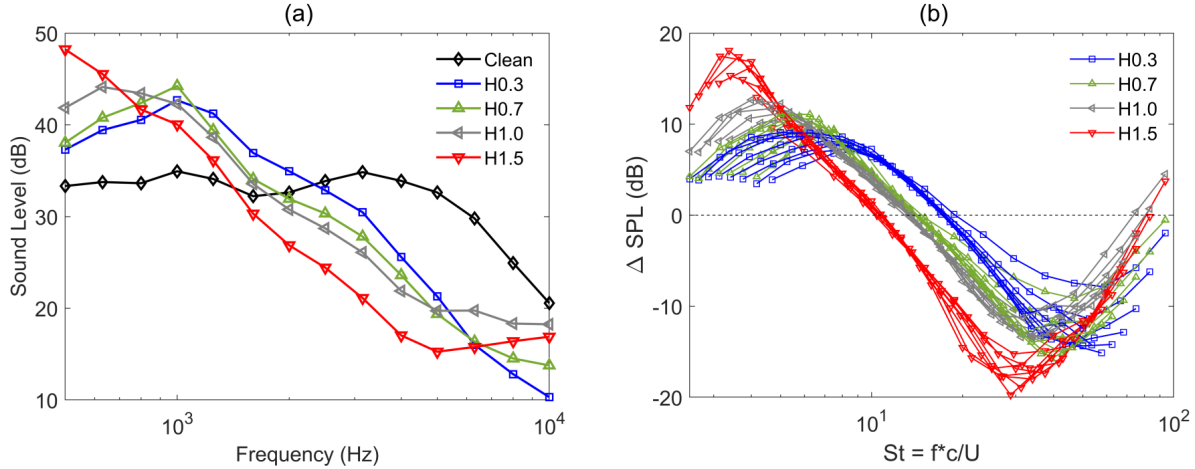


Fig. 5 (a) Corrected Sound Level within the trailing edge integration contour for different velvety coatings at 20 m/s. (b) The difference of trailing edge noise between the coated configuration and the clean configuration, as a function of chord based Strouhal number at 16-30 m/s. Positive ΔSPL represents noise addition, while negative ΔSPL represents noise reduction.

noise becomes more apparent in the acoustic image. For the H1.5 configuration, the modification of the acoustic source distribution is even more significant. At 2,000 Hz, the maximum source strength at the trailing edge is already reduced by around 6 dB compared to the clean configuration. At 4,000 and 8,000 Hz, it is clear that the dominant noise source is not distributed in the trailing edge region, and more substantial noise reduction was achieved compared to the H0.3 velvety coating.

The absolute sound level of the trailing edge noise within each third-octave band was calculated using the source integration method. The integration contour covers the centre 25% of the span and $\pm 75\%$ of the chord with respect to the trailing edge, as indicated in Fig. 4. The duplicate summation caused by the point spread function of the microphone array was corrected by an Array Calibration Function (ACF) [31]. Simulated microphone signals of incoherent monopoles distributed evenly along the flat plate trailing edge were generated to model the trailing edge noise [32]. The source distribution was reconstructed using the simulated signals and the beamforming algorithm, and the sound level was calculated from the source integration method, which was then compared to the actual source level to give the ACF.

After the correction by ACF, the absolute sound levels within the trailing edge integration contour for different configurations at 20 m/s are plotted in Fig. 5(a). The effect of velvety coatings on the trailing edge noise is largely frequency-dependent. For each velvety coating, there is a critical frequency f_{crit} , below which the coating increases the trailing edge noise, while above f_{crit} the trailing edge noise is reduced. The effect of velvety coating for frequency above 10,000 Hz was not determined, due to the upper limit of the frequency response of the microphone. The hair dimension affects both the critical frequency and the magnitude of noise addition/reduction. Compared to other velvety coatings, the coating H1.5 gives a lower f_{crit} , and a higher noise reduction for most of the frequencies above f_{crit} . However, it also gives higher noise increment in the low-frequency range.

Figure 5(b) includes the effect of the flow speed by using chord-based Strouhal number $St = f \cdot c/U$ as the abscissa axis. All the measurement results with the free stream velocity between 16 m/s to 30 m/s are plotted. The change of trailing edge noise ΔSPL caused by the coating is found to be a quantity to achieve good data collapse. The critical Strouhal number St_{crit} corresponding to f_{crit} appears to be nearly invariant within the measured speed range. The St_{crit} for H0.3, H0.7, H1.0 and H1.5 velvety coating are 17.5, 14.0, 13.3 and 10.5, respectively, indicating that St_{crit} is negatively related to the length of the velvety coating. When the Strouhal number is smaller than the critical value St_{crit} , the significant noise increment is possibly due to the blunt trailing edge vortex shedding noise, since the trailing edge thickness-based Strouhal number $St_h = f \cdot h/U$ for the peak is around 0.1 for all of the coatings. This peak Strouhal number St_h is consistent with the results for the blunt trailing edge noise in the study by Herr and Dobrzynski [33]. In the high Strouhal number range, the noise is largely reduced possibly because the velvety coating shields the sharp trailing edge from the small vortex structures in the turbulent boundary layer, therefore suppresses the trailing edge scattering. The reason why the thicker velvety coating gives a smaller St_{crit} and more effective noise reduction at high-frequency is possibly because the thicker velvety coating is able to reject larger vortices from the hard surface

underneath. However, more quantitative analysis and experimental validation are required to verify this conjecture.

2. Effect of the location of the velvety structure

Further measurements were conducted to investigate the effect of the velvety coating location on the trailing edge noise. The velvety coating with 1 mm hair length was used in this section. The velvety coating has 100% spanwise and 36.7% chordwise length, and was adhered to different chordwise locations, as summarized in Table 2. For the H1.0_P1 configuration, the downstream end of the velvety coating was aligned with the trailing edge. For the remaining configurations, the velvety coating was moved upstream the trailing edge, giving a non-coated region near the trailing edge. All of these configurations have symmetric coatings on both sides of the flat plate model.

Table 2 Different locations of the partially covered velvety coatings.

Configuration	H1.0_P1	H1.0_P2	H1.0_P3	H1.0_P4	H1.0_P5
Distance from TE (mm)	0	10	20	30	55

Figure 6 shows the beamforming results for the clean configuration and two of the five partially coated configurations at 20 m/s flow speed. It is clear from the figure that the velvety coating is more effective in reducing high frequency trailing edge noise when put closer to the trailing edge. When the coating is far upstream the trailing edge (H1.0_P5), distinct trailing edge noise is clearly visible in the acoustic image, although the magnitude of the source intensity is slightly reduced. The source integration results in Fig 7(a) show that the distance between the coating to the trailing edge has a monotonic effect on the trailing edge noise intensity. The coating is most effective in reducing high-frequency noise when it covers the trailing edge. When the coating is shifted upstream, the noise reduction ability at high frequency weakens. However, the substantial noise reduction at high frequency also comes with a penalty of enhanced noise at low frequency. This is similar to the conclusion from the last section. From Fig 7(b), one can observe that for each configuration, the effect of the velvety coating on the trailing edge noise is similar at different flow speeds. The critical Strouhal number St_{crit} is found to be negatively related to the distance between the coating and the trailing edge.

B. Flow measurement results

Served as a supplementary measurement, the flow measurement was only conducted for the clean, H0.3 and H1.5 configurations. The mean and root mean square (RMS) velocity distribution at 0.7mm downstream the trailing edge are shown in Fig. 8. Both distributions have good symmetry, which proves good model installation accuracy. In terms of the mean velocity, it is clear that the velvety coating broadens the boundary layer thickness, compared to the clean configuration. The 1.5 mm thick velvety coating has a larger broadening effect than the 0.3 mm thick coating. In addition, for the H1.5 configuration, there clearly exists a region near the trailing edge ($y = 0$) where the mean velocity is small and nearly constant. This is likely due to the large bluntness caused by the thick coating. The velvety coating also widens the regions with high fluctuating velocity, with thicker coating having larger effect. However, the maximum magnitude of the RMS velocity remains similar in all three cases.

The spectral density of the fluctuation velocity of the above three cases are plotted in Fig. 9. It is clear that all three spectra are broadband, which confirms that the flow at the trailing edge is turbulent. For the clean configuration, the turbulent energy is concentrated at the low frequency and within the boundary layer. For the H0.3 and H1.5 configuration, there are two major differences from the clean configuration. First, the width of the region with high velocity spectrum is increased. Second, there is a wider region of low velocity spectrum around $y = 0$. It is clear that the high-frequency velocity fluctuation is reduced at this centre zone, compared to the clean configuration. The increased width of this region can be attributed to the increased trailing edge bluntness caused by the coating.

In order to focus on the overall turbulent energy distribution in the whole boundary layer, integration of the turbulent spectrum was conducted in the y -direction (see Fig. 10). Both velvety coatings consistently elevate the integrated turbulent spectrum in the whole frequency range, and the thicker coating H1.5 gives larger increment. This can be mainly attributed to the extra surface roughness associated with the artificial velvety coating.

C. Connections between the noise and flow measurements

According to the flow measurement results, the turbulent spectrum in the boundary layer is increased at all frequencies by the application of the artificial velvety coating. If the trailing edge scattering mechanism remains the same, then

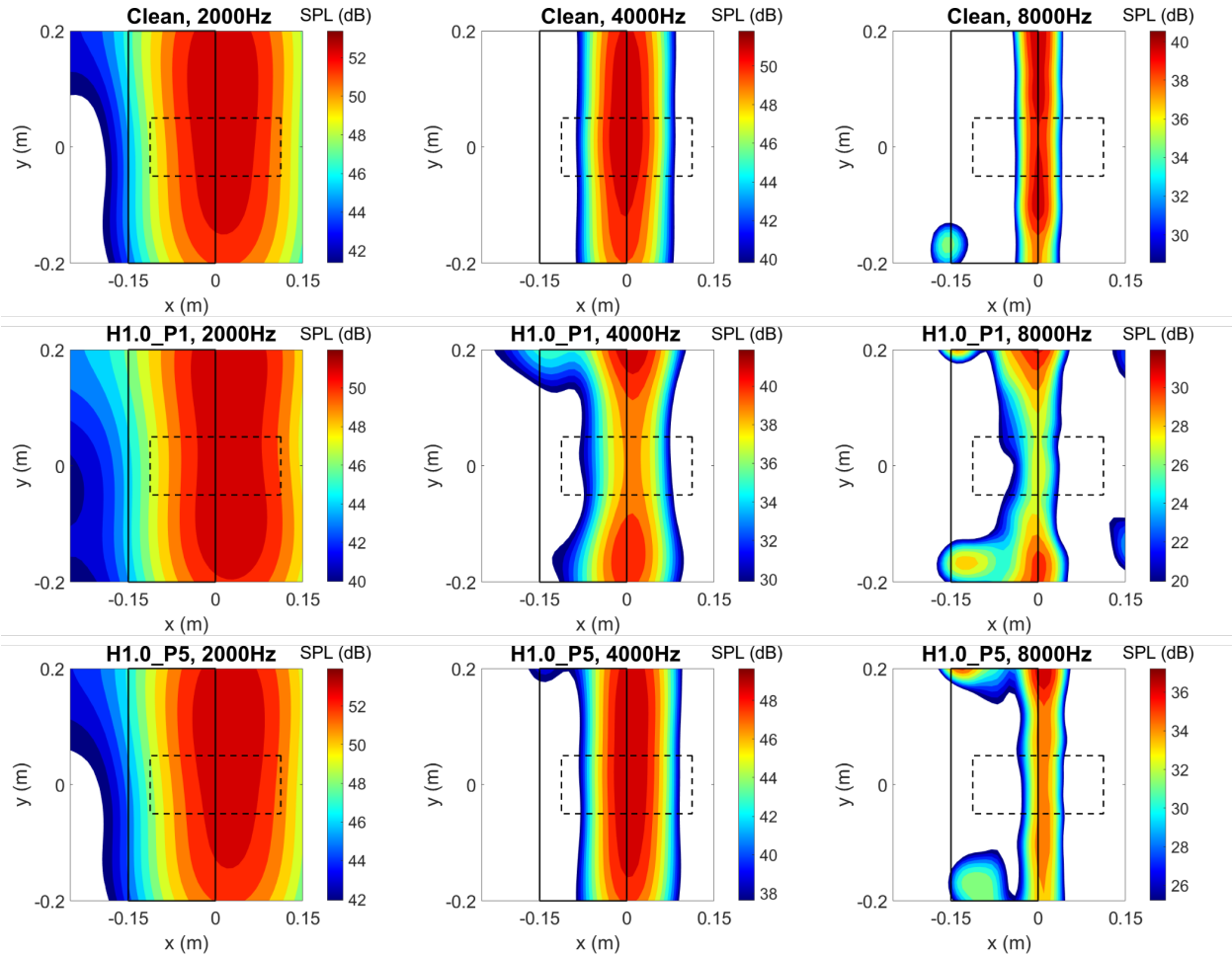


Fig. 6 Comparison of the 1/3-octave acoustic images at three different frequencies. Upper row: clean flat plate model; middle row: flat plate model partially coated with 1.0 mm coating (H1.0_P1); lower: flat plate model partially coated with 1.0 mm coating (H1.0_P5). Flow direction is from left to right. The solid contour indicates the flat plate model, and the dashed contour indicates the integration region. The dynamic range of the color scale is 12 dB.

the velvety coating should increase the trailing edge noise at all frequencies, which does not agree with the noise measurement result. It is possible that the velvety coating does not reduce the overall turbulent energy, as proposed by Lilley [7], but only modifies the spatial distribution of the turbulent energy. From Fig. 9 it is clear that for the H1.5 configuration, the velocity spectrum at the trailing edge ($y = 0$) at high frequency is reduced, compared to the clean configuration. This supports the conjecture that the velvety coating shields the sharp trailing edge from small eddies with high frequency, in other words, modifies the overall trailing edge scattering efficiency.

D. Biological significances

It would be interesting to relate the experimental condition with the real owl flight condition. Take the barn owl as an example. According to Bachmann [34], the mean chord of the barn owl's wing is typically around 17 cm, and the thickness of the velvety structure on the upper wing surface is around 0.3–1 mm. These parameters are very close to those in this experimental study. If the experimental results are extended to the case of the barn owl's flight, then the velvety structure can achieve noise reduction above a chord-based Strouhal number of around 17. Because the normal flight speed of the barn owl during hunting is less than 10 m/s, the associated f_{crit} is approximately 1 kHz. Hence, a reduction in flight noise above 1 kHz is expected. Owls' preys, on the other hand, are only sensitive to the sound well above 2 kHz, according to the hearing curve provided by Neuhaus *et al.* [6]. Therefore, the sound reduction at high

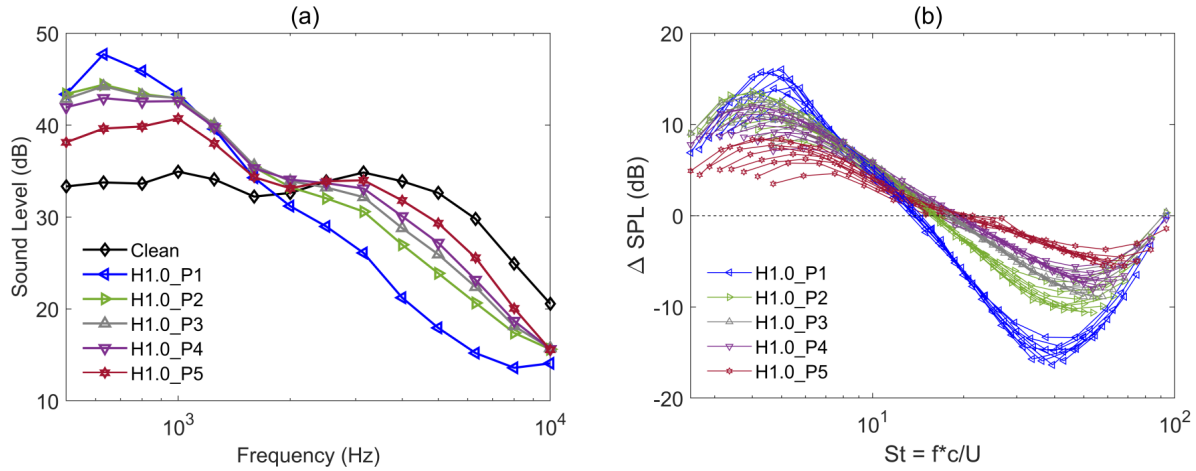


Fig. 7 (a)Corrected Sound Level within the trailing edge integration contour for the clean and partially coated configurations at 20 m/s. (b)The change of trailing edge noise compared to the clean configuration achieved by different velvety coatings as a function of chord based Strouhal number at 16-30 m/s. Positive Δ SPL represents noise addition.

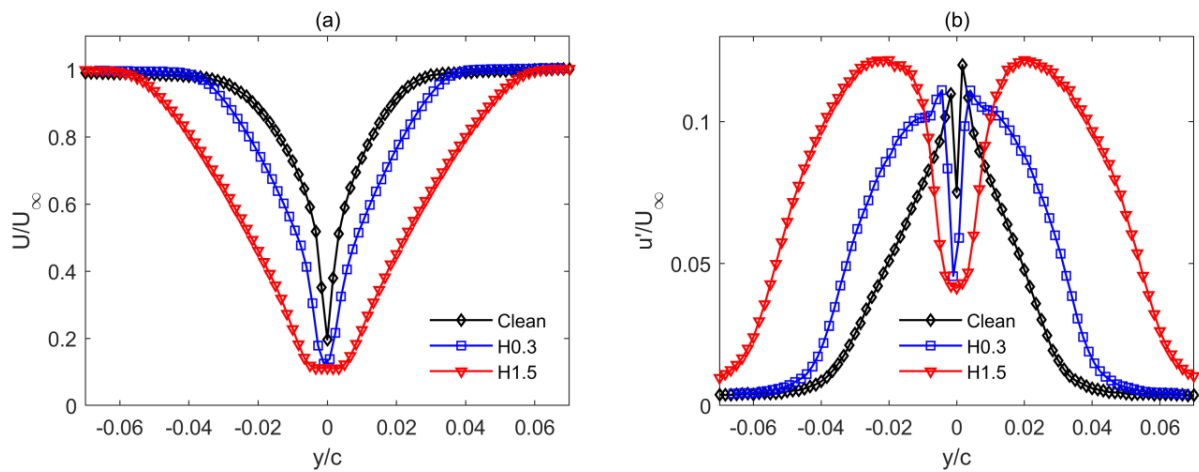


Fig. 8 Mean velocity distribution (a) and RMS velocity distribution (b) at 0.7 mm downstream the trailing edge. The free stream velocity is 20 m/s.

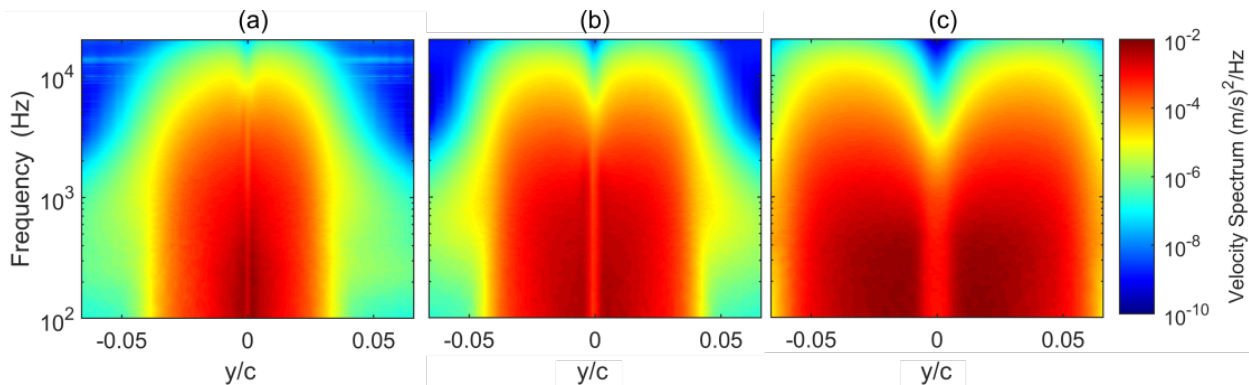


Fig. 9 The spectral density of the fluctuating velocity component, u' , at different y , for (a):clean configuration, (b): H0.3 configuration and (c): H1.5 configuration. The free stream velocity is 20 m/s.

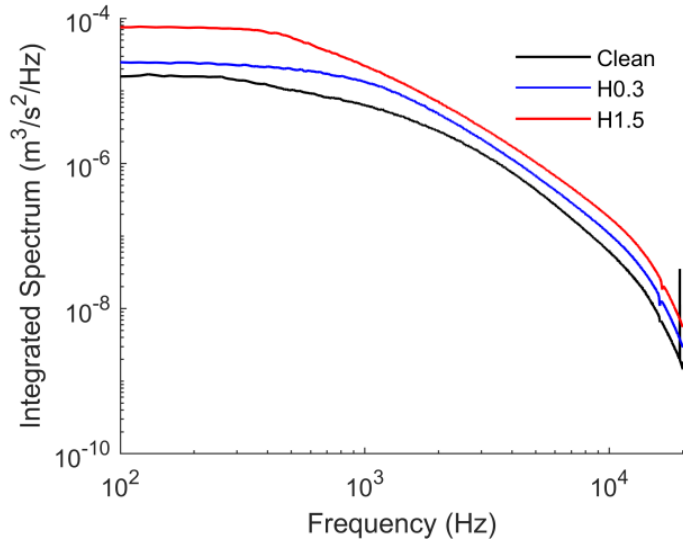


Fig. 10 The integral of the velocity spectral density along the y direction for three testing configurations.

frequencies by the velvety structure might be dominant.

V. Conclusions

This paper attempts to investigate the contribution of the velvety structure on owls' feather to owls' quiet flight. To achieve a controlled aeroacoustic study, four types of artificial velvety coatings were fabricated to mimic the microscopic structure and mechanical properties of the natural velvety structure on owls' feather, and were attached to a tripped flat plate model. The effect of the thickness and location of the velvety coating on trailing edge noise was experimentally investigated through an anechoic wind tunnel testing with a phased microphone array. Acoustic beamforming results show that for the clean flat plate model, the dominant noise sources at mid-to-high frequencies are distributed along the trailing edge. The attached velvety coating can significantly modify the acoustic source distribution and the intensity of the trailing edge noise. For each coating, there is a critical Strouhal number St_{crit} , above which the noise is reduced, while below which the noise is increased. Both the thickness and the location of the velvety coating affect the trailing edge noise spectrum. A thicker coating results in a smaller St_{crit} , larger noise reduction at high frequencies, and larger noise addition at low frequencies. Moving the coating upstream increases the St_{crit} , reduces the noise reduction at high frequencies, and reduces the noise increment at low frequencies.

Flow measurement results show that the artificial velvety coating consistently increases the overall velocity spectrum in the boundary layer at all frequencies. However, at the location near the trailing edge, the velocity fluctuation is reduced, especially for the high-frequency components. Therefore, it is suspected that the major mechanism for the high-frequency noise reduction is that the velvety coating shields the trailing edge from small turbulent eddies with high frequencies.

Three hypotheses regarding the function of the velvety structure on owls' quiet flight were addressed in the study. Firstly, the sound absorption by the velvety structure is measured to be non-essential to the quiet flight. Secondly, it is likely that the velvet modifies the trailing edge scattering mechanism. Lastly, the velvet may not absorb the high-frequency turbulent fluctuations, but only change the spatial distribution of the boundary layer turbulence.

Acknowledgments

Peng Zhou wishes to thank The Hong Kong University of Science and Technology (HKUST) and Hong Kong RGC PhD Fellowship (reference number: PF16-01286) for supporting part of the PhD thesis research. This work was performed in Aerodynamics, Acoustics & Noise control Technology Centre (aantc.ust.hk).

References

- [1] Lockard, D. P., and Lilley, G. M., "The airframe noise reduction challenge," Tech. rep., NASA-TM-2004-213013, 2004.
- [2] Williams, J. F., and Hall, L., "Aerodynamic sound generation by turbulent flow in the vicinity of a scattering half plane," *Journal of Fluid Mechanics*, Vol. 40, No. 4, 1970, pp. 657–670.
- [3] Amiet, R. K., "Noise due to turbulent flow past a trailing edge," *Journal of Sound and Vibration*, Vol. 47, No. 3, 1976, pp. 387–393.
- [4] Graham, R., "The silent flight of owls," *The Aeronautical Journal*, Vol. 38, No. 286, 1934, pp. 837–843.
- [5] Fowler, M., and Cubas, Z. S., *Biology, medicine, and surgery of South American wild animals*, John Wiley & Sons, 2008.
- [6] Neuhaus, W., Bretting, H., and Schweizer, B., "Morphologische und funktionelle Untersuchungen über den "lautlos" Flug der Eulen (*Strix aluco*) im Vergleich zum Flug der Enten (*Anas platyrhynchos*)," *Biol Zbl*, Vol. 92, 1973, pp. 495–512.
- [7] Lilley, G., "A study of the silent flight of the owl," *AIAA Paper 1998-2340, 4th AIAA/CEAS aeroacoustics conference*, Toulouse, France, 1998.
- [8] Payne, R. S., "Acoustic location of prey by barn owls (*Tyto alba*)," *Journal of Experimental Biology*, Vol. 54, No. 3, 1971, pp. 535–573.
- [9] Dyson, M., Klump, G., and Gauger, B., "Absolute hearing thresholds and critical masking ratios in the European barn owl: a comparison with other owls," *Journal of Comparative Physiology A: Neuroethology, Sensory, Neural, and Behavioral Physiology*, Vol. 182, No. 5, 1998, pp. 695–702.
- [10] Kroeger, R. A., Grushka, H. D., and Helvey, T. C., "Low speed aerodynamics for ultra-quiet flight," Tech. rep., AFFDL-TR-71-75, Air Force Flight Dynamics Laboratory, 1972.
- [11] Gruschka, H., Borchers, I., and Coble, J., "Aerodynamic noise produced by a gliding owl," *Nature*, Vol. 233, No. 5319, 1971, pp. 409–411.
- [12] Howe, M. S., *Theory of vortex sound*, Vol. 33, Cambridge University Press, 2003.
- [13] Sarradj, E., Fritzsche, C., and Geyer, T., "Silent owl flight: bird flyover noise measurements," *AIAA Journal*, Vol. 49, No. 4, 2011, pp. 769–779.
- [14] Wagner, H., Weger, M., Klaas, M., and Schröder, W., "Features of owl wings that promote silent flight," *Interface Focus*, Vol. 7, No. 1, 2017, p. 20160078.
- [15] Bachmann, T., Klän, S., Baumgartner, W., Klaas, M., Schröder, W., and Wagner, H., "Morphometric characterisation of wing feathers of the barn owl *Tyto alba* pratincola and the pigeon *Columba livia*," *Frontiers in Zoology*, Vol. 4, No. 1, 2007, p. 23.
- [16] Chen, K., Liu, Q., Liao, G., Yang, Y., Ren, L., Yang, H., and Chen, X., "The sound suppression characteristics of wing feather of owl (*Bubo bubo*)," *Journal of Bionic Engineering*, Vol. 9, No. 2, 2012, pp. 192–199.
- [17] Vad, J., Kosco, G., Gutermuth, M., Kasza, Z., Tábi, T., and Csörgo, T., "Study of the aero-acoustic and aerodynamic effects of soft coating upon airfoil," *JSME International Journal Series C Mechanical Systems, Machine Elements and Manufacturing*, Vol. 49, No. 3, 2006, pp. 648–656.
- [18] Klän, S., Burgmann, S., Bachmann, T., Klaas, M., Wagner, H., and Schröder, W., "Surface structure and dimensional effects on the aerodynamics of an owl-based wing model," *European Journal of Mechanics-B/Fluids*, Vol. 33, 2012, pp. 58–73.
- [19] Winzen, A., Klaas, M., and Schröder, W., "High-speed particle image velocimetry and force measurements of bio-inspired surfaces," *Journal of Aircraft*, Vol. 52, No. 2, 2014, pp. 471–485.
- [20] Clark, I., Devenport, W. J., Jaworski, J., Daly, C., Peake, N., and Glegg, S. A., "The noise generating and suppressing characteristics of bio-inspired rough surfaces," *AIAA Paper 2014-2911, 20th AIAA/CEAS aeroacoustics conference*, Atlanta, GA, USA, 2014.
- [21] Clark, I. A., Alexander, W. N., Devenport, W., Glegg, S., Jaworski, J. W., Daly, C., and Peake, N., "Bioinspired trailing-edge noise control," *AIAA Journal*, Vol. 55, No. 3, 2016, pp. 740–754.
- [22] Lingham-Soliar, T., "Feather structure, biomechanics and biomimetics: the incredible lightness of being," *Journal of ornithology*, Vol. 155, No. 2, 2014, pp. 323–336.

- [23] Bachmann, T., Emmerlich, J., Baumgartner, W., Schneider, J. M., and Wagner, H., "Flexural stiffness of feather shafts: geometry rules over material properties," *Journal of Experimental Biology*, Vol. 215, No. 3, 2012, pp. 405–415.
- [24] Gao, J., Chu, J., Guan, L., and Zhang, R., "Mechanical properties and size scaling of long-eared owl primary feather," *International Journal of Materials and Structural Integrity*, Vol. 11, No. 1-3, 2017, pp. 32–50.
- [25] Bu, H., Yu, W., Kwan, P.-W., and Huang, X., "Wind-tunnel investigation on the compressive-sensing technique for aeroengine fan noise detection," *AIAA Journal*, Vol. 56, No. 9, 2018, pp. 3536–3546.
- [26] Zhou, T., Sun, Y., Fattah, R., Zhang, X., and Huang, X., "An experimental study of trailing edge noise from a pitching airfoil," *The Journal of the Acoustical Society of America*, Vol. 145, No. 4, 2019, pp. 2009–2021.
- [27] Doolan, C., Tetlow, M., Moreau, D., and Brooks, L., "Vortex shedding and tonal noise from a sharp bevelled trailing edge," *AIAA Paper 2012-68, 50th AIAA Aerospace Sciences Meeting including the New Horizons Forum and Aerospace Exposition*, Nashville, TN, USA, 2012.
- [28] Huang, X., "Real-time location of coherent sound sources by the observer-based array algorithm," *Measurement Science and Technology*, Vol. 22, No. 6, 2011, p. 065501.
- [29] Sijtsma, P., "Phased array beamforming applied to wind tunnel and fly-over tests," Tech. rep., NLR-TP-2010-549, 2010.
- [30] Oerlemans, S., and Migliore, P., "Aeroacoustic wind tunnel tests of wind turbine airfoils," *AIAA Paper 2004-3042, 10th AIAA/CEAS Aeroacoustics Conference*, Manchester, Great Britain, 2004.
- [31] Brooks, T., and Humphreys, W., Jr., "Effect of directional array size on the measurement of airframe noise components," *AIAA Paper 1999-1958, 5th AIAA/CEAS Aeroacoustics Conference and Exhibit*, Bellevue, WA, USA, 1999.
- [32] Oerlemans, S., and Sijtsma, P., "Determination of absolute levels from phased array measurements using spatial source coherence," *AIAA Paper 2002-2464, 8th AIAA/CEAS Aeroacoustics Conference & Exhibit*, Breckenridge, CO, USA, 2002.
- [33] Herr, M., and Dobrzynski, W., "Experimental investigations in low-noise trailing-edge design," *AIAA Journal*, Vol. 43, No. 6, 2005, pp. 1167–1175.
- [34] Bachmann, T. W., "Anatomical, morphometrical and biomechanical studies of barn owls' and pigeons' wings," Ph.D. thesis, RWTH Aachen University, Germany, May 2010.